Journal of the Optical Society of Korea, Vol. 7, No. 2, June 2003, pp. 79-83

The Fabrication of a Photonic Crystal Fiber and Measurement of its Properties

Jinchae Kim*, Ho Kyung Kim, Un-Chul Paek, and Byeong Ha Lee

Department of Information and Communications, Kwangju Institute of Science and Technology, Gwangju 500-712, KOREA

Joo Beom Eom

Korea Photonics Technology Institute, Gwangju 500-210, KOREA

(Received April 4, 2003)

In this paper, we describe the fabrication process of a photonic crystal fiber and present the measured optical properties of the photonic crystal fiber. The fabrication of the photonic crystal fiber involves stacking, jacketing, collapsing, and drawing using a conventional drawing tower. The photonic crystal fiber drawing needs higher tension to maintain the uniform air hole structure. Thus, the temperature of the photonic crystal fiber drawing is lowered by a few hundred degrees Celsius than for the case of conventional optical fiber drawing. The optical properties of the fabricated photonic crystal fiber such as mode profile, optical loss, transmission spectrum, bending loss, and polarization dependent loss are measured.

OCIS codes : 060.0060, 060.2400.

I. INTRODUCTION

Photonic crystal fiber (PCF) [1], also known as holey fiber [2](see Fig. 1), is made by single material unlike the conventional optical fiber, in which materials of different refractive indices are used for core and cladding. The PCF normally consists of a regular pattern of tiny air holes inside pure silica in the transverse direction and along the longitudinal direction. The PCF has recently caught much attention because of its unusual optical characteristics such as single mode operation over a wide wavelength range [1], large mode field diameter [3], tailorable dispersion by air hole structure [2,4–7], nonlinear effects [8,9], grating [10], and birefringence [11]. These properties enable PCF to be used in novel devices such as PCF

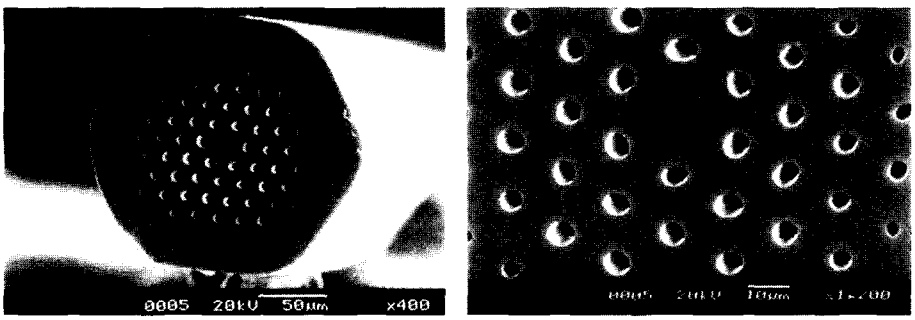

(a) (b)

FIG. 1. The SEM pictures of the cleaved facet of the PCF (a) and its magnified view (b).

coupler [12], the medium for supercontinuum generation [13,14], lasers, and sensor applications. The optical characteristics of the PCF can be tailored by changing the structure and dimension of air holes. The fabrication of the PCF is more difficult than that of solid fiber, because the PCF has many tiny air holes through the cross-section of PCF unlike the conventional solid fiber. Thus, special techniques such as high tension drawing are required to make the PCF with uniform air hole structure.

In this paper, we describe the fabrication method of the PCF preforms and the drawing process. The measured optical properties of the PCF such as mode profile, loss, transmission spectrum, bending loss, and polarization dependent loss are also presented.

II. FABRICATION

The fabrication procedure of the PCF preform is somewhat different compared to the conventional optical fiber preform, which is made by MCVD, VAD, OVD *etc*, due to the air hole structure of the PCF.

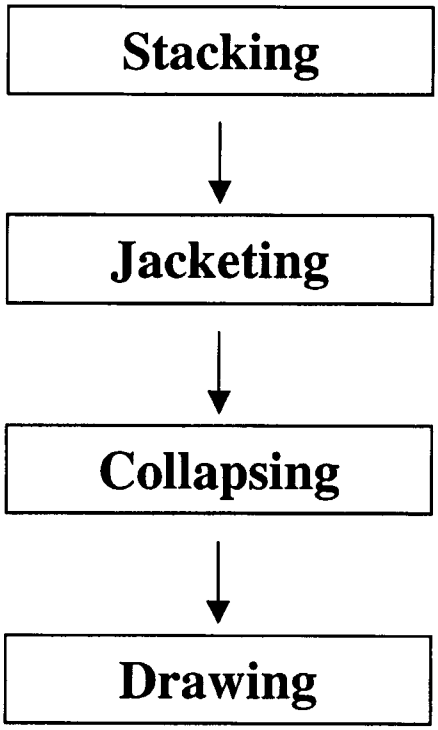

FIG. 2. Fabrication flow-chart of the PCF with the stacking-and-drawing method.

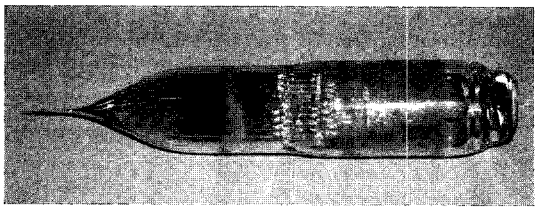

FIG. 3. Side view of the preform of the PCF after stacking, jacketing, and collapsing.

Fig. 2 shows the flow-chart, which describes the sequence of procedures involved in making the preform and drawing PCFs. The preform fabrication process involves stacking of tubes, jacketing, and collapsing using the lathe of the MCVD to maintain the structure. The PCF drawing is conducted using a conventional drawing tower. In the stacking, many pure silica tubes (3×2 mm) are located around a rod(s) (3 mm) at the center. Even though we used epoxy and nichrome wire to tie the bundle together, oxy-hydrogen torch can also be used for the same purpose. In order to protect the bundle of the tubes, jacketing with a big tube (34×38 mm) and collapsing process are needed. The jacketing and collapsing process are carried out in the lathe of the MCVD process. The fabricated preform of PCF is shown in Fig. 3. In general, the diameter of the preform is about 36 mm and the length is 30−100 cm. The PCF is also fabricated by the conventional drawing tower. In the initial stage of the drawing, a high temperature of about 2150 °C, which is the furnace temperature for the drawing of conventional optical fiber, is required to lower the fiber tension to cover the polymer coating on the fiber surface and to wind the fiber on the spool. The air holes of the fiber will be closed due to low tension and low viscosity at high temperature. The furnace temperature is lowered below 2000 °C after the polymer coating and winding process are initiated. Air hole formation is difficult at the high temperature due to lack of enough tension. The fiber tension can be increased, either by decreasing the furnace temperature or/and increasing the fiber drawing speed. Suitable tension on the fiber is required to fabricate the PCF with uniform air hole structure. When too much tension is loaded on the fiber, the fiber may break during the drawing. This is the reason why good PCF is hard to make. The structural change in the fiber during the drawing is shown in Fig. 4 after lowering the furnace temperature to about 1980 °C, and the drawing speed of 17 m/min. Figs. 4(a), (b), and (c) are cut-view of the fiber with time step of 10 min. It takes about 30 minutes to obtain good-shaped PCF after stabilizing the temperature at 1980 °C. By increasing the drawing

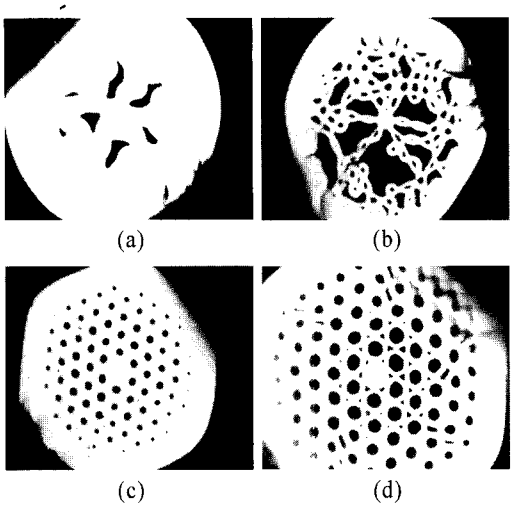

FIG. 4. A series of cut-view images of the PCF under drawing. During the drawing process the images were taken every 10 minutes (10 (a), 20 (b) and 30 min (c)), and then higher tension was applied to enlarge the diameter of air holes (d).

speed, *i.e.*, increasing tension, the PCF with larger diameter of the air hole can be obtained as shown in Fig. 4(d) while still maintaining the diameter of about 125 μm.

Even though they are fabricated from the same preform, Fig. 4(d) and the inset of Fig. 5 show the unwanted interstitial air holes of the PCF and partially or completely collapsed air hole layer(s) respectively, while the PCF in Fig. 4(c) shows uniform air hole structure. It is well known that, the temperature affects the viscosity according to the Arrenius-type equation and the viscosity is also proportional to the drawing tension [15]. The temperature distribution inside the preform is non-uniform along the transverse direction as well as the longitudinal direction due to the difficulty of the heat transfer to the inside of the preform, and the furnace temperature distribution [16]. The air holes in the preform hinder the heat transfer from reaching the inner layer of the preform and hence the inner layer of the preform experiences lower temperatures leading to higher viscosity (or surface tension) in the inner layer of the preform. Thus the air holes at the outer layer of the preform tend to collapse more easily compared to those of inner.

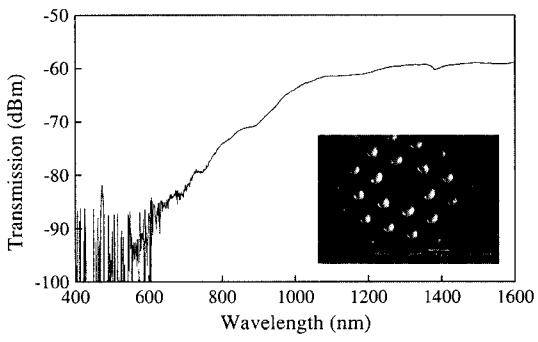

FIG. 5. Transmission spectrum of the fabricated PCF. The diameter of air hole and its distance are 4.5 μm and 10.2 μm, respectively.

III. MEASUREMENT

The basic optical properties of the PCF such as optical loss, near field, macrobending loss, transmission spectrum, and polarization dependent loss were measured. The transmission spectrum is shown in Fig. 5. The inset in Fig. 5 is the cross-sectional view of the measured PCF whose dimension is 4.5 μm diameter of air hole and 10.2 μm hole-to-hole distance. The optical loss at a wavelength of 1.55 μm was measured to be about 0.2 dB/m, which is quite low compared to our first reported PCF [12]. The decrease in the loss can be due to the reduction in the total dimension of the PCF. The PCF with the small dimension is less sensitive to the unwanted bending, which occurs during the measurement [1,17].

The near field image was captured by a Vidicon camera with different laser sources. The PCF sample, several tens of centimeters long, was prepared for the polymer coating, whose refractive index was larger than that of the fused silica. Fig. 6 shows the near field images at 635 (a) and 1550 nm (b) wavelengths.

At a longer-wavelength, the modal field is well confined in the solid core region, but the field at a shorter-wavelength is largely spread into the silica of the holey cladding region with inevitable small bending during the measurement. At the shorter-wavelength the amount of the evanescent field, existing inside the air holes in the holey cladding region, is small compared to that at the longer-wavelength. At the shorter-wave-

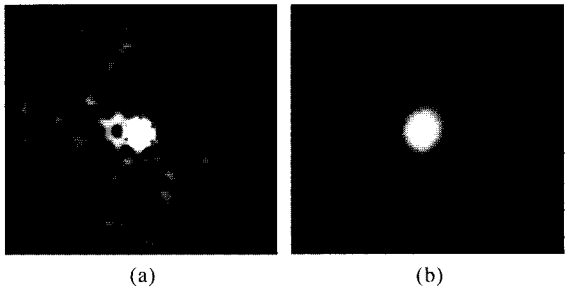

FIG. 6. Near field images of the PCF measured at the wavelength of 635 (a) and 1550 nm (b).

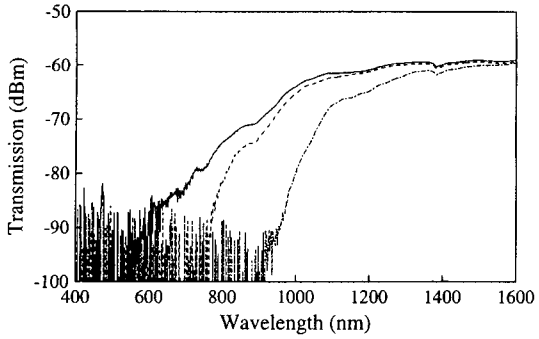

FIG. 7. Transmission spectra with various bending radii of infinite (solid), 6 (dash), and 3 cm (dash-dot).

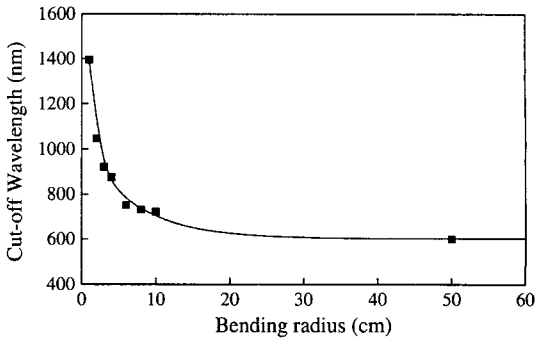

FIG. 8. Cut-off wavelength variation plotted in terms of the bending radius (squared). The solid line is the fitted line by double exponential function.

length, it feels lower effective index difference between the solid core and the holey cladding region [18]. That means the light can not distinguish between the central silica defect(s) and the silica in the holey cladding. So the light at shorter-wavelengths is more susceptible to bending than that at longer-wavelengths. This is one of the reasons why the optical loss at a shorter-wavelength is larger than that at a longer-wavelength in the fabricated PCF as seen in Fig. 5.

In order to study the guiding properties of light in PCF, we performed macrobending experiments. The measurement of the macrobending characteristics of the PCF was taken by the single-turn radius method, in which a white-light source (Ando AQ4303B) and an OSA (Ando AQ6317B) were used. The length of the PCF used for the experiment was about 1 m. Fig. 7 shows the transmission spectra of the PCF measured with different bending radii of 3, 6 cm, and infinity. In the case of an infinite bending radius, the cut-off wavelength was about 600 nm and was found to be increased by decreasing the radius. The cut-off wavelengths were 750 and 920 nm for bending radii of 6 and 3 cm, respectively. Fig. 8 shows the variation of the cut-off wavelength of the PCF with the bending radius.

Fig. 7 shows that, as the bending radius becomes smaller, the cut-off wavelength of the mode shifts to the longer-wavelength. This means the macrobending limits the light propagation in the PCF at the shorter-wavelength. Fig. 8 shows the cut-off wavelength variation with bending radius. The squared points represent the measured values, while solid line is the fit of the data. The unwanted bending may add to the error in the measurement. The cut-off wavelength for infinite bending radius is measured to be about 600 nm. Because of the flat behavior of the curve, we indicated the infinite bending radius point at 0.5 m.

We define the critical bending radius as the radius at which the cut-off wavelength just starts to increase. The critical bending radius mainly depends on the structure of the PCF, such as hole-to-hole distance, hole diameter, and the wavelength [1]. The critical bending radius increases with the hole-to-hole distance and decreases with wavelength [1].

The polarization dependent loss (PDL) was measured by using the IQ12004B DWDM Passive Component Test system of EXFO Incorporation [19]. It uses the Mueller matrix method to measure the PDL of the device under test over the wavelength range of 1510 nm to 1610 nm. The length of the fabricated PCF for PDL measurement was about 2 m. In the same experimental condition, PDL of the PCF (bold line in Fig. 9) is larger by about 30 mdB than that of conventional single-mode fiber (dotted line, $\Delta \sim 0.5$ %, core diameter ~ 9 μm).

IV. SUMMARY

The PCF preform was fabricated by stacking many capillary tubes, then jacketing and collapsing it with

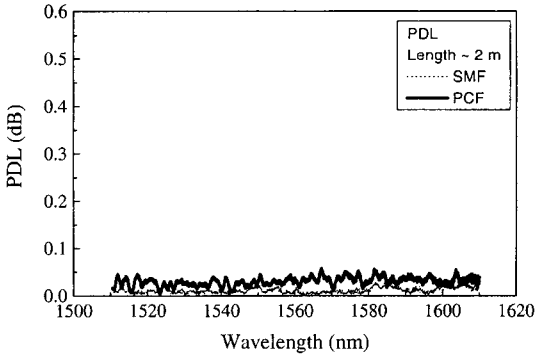

FIG. 9. Polarization dependent loss of the PCF (bold line) and SMF (dotted line). The lengths of both fibers were about 2 m.

a big tube to protect the structure of the capillary tubes. The PCF was drawn by a conventional drawing tower with furnace temperature below 2000 °C, which is lower than that used for conventional solid fiber drawing. The various optical properties such as optical loss, near field, macrobending induced loss, transmission spectrum, and polarization dependent loss were measured. The near field image shows good guidance at the wavelength of 1.55 μm. The transmission loss of the fabricated PCF was about 0.2 dB/m at the C-band. The macrobending induced loss of the fabricated PCF may limit the light propagation at shorter-wavelengths. The polarization dependent loss of the PCF was somewhat higher than that of conventional step-index single-mode fiber.

ACKNOWLEDGEMENTS

This work was partially supported by KOSEF through UFON, an ERC Program, and by Brain Korea 21 Program of MOE, Korea.

*Corresponding author : jeicy@kjist.ac.kr.

REFERENCES

[1] J. C. Knight, T. A. Birks, and P. St. J. Russell, "Endlessly single-mode photonic crystal fiber," *Opt. Lett.*, vol. 22, no. 13, pp. 961–963, 1997.

[2] T. M. Monro, D. J. Richarson, N. G. R. Broderick, and P. J. Bennett, "Holey optical fibers: An efficient modal model," *IEEE J. Lightwave Technol.*, vol. 17, no. 6, pp. 1093–1102, 1999.

[3] J. C. Knight, T. A. Birks, R. F. Cregan, P. St. J. Russell, and J. P. de Sandro, "Large mode area photonic crystal fibre," *Electron. Lett.*, vol. 34, no. 13, pp. 1347–1348, 1998.

[4] T. A. Birks, D. Mogilevtsev, J. C. Knight, and P. St. J. Russell, "Dispersion compensation using single-material fibers," *IEEE Photon. Technol. Lett.*, vol. 11, no. 6, pp. 674–676, 1999.

[5] M. J. Gander, R. McBride, J. D. C. Jones, D. Mogilevtsev, T. A. Birks, J. C. Knight, and P. St. J. Russell, "Experimental measurement of group velocity dispersion in photonic crystal fiber," *Electron. Lett.*, vol. 35, no. 1, pp. 63–64, 1999.

[6] D. Mogilevtsev, T. A. Birks, and P. St. J. Russell, "Group-velocity dispersion in photonic crystal fibers," *Opt. Lett.*, vol. 23, no. 21, pp. 1662–1664, 1999.

[7] J. Kim, U.-C. Paek, D. Y. Kim, and Y. Chung, "Analysis of the dispersion properties of holey optical fibers using normalized dispersion," *in Optical Fiber Communication Conference* vol. 54 of OSA Trends in Optics and Photonics Series (Optical Society of America, Washington, D.C., 2001), WDD86.

[8] W. J. Wadsworth, J. C. Knight, A. Ortigosa-Blanch, J. Arriaga, E. Silvestre, and P. St. J. Russell, "Soliton effects in photonic crystal fibres at 850 nm," *Electron. Lett.*, vol. 36, no. 1, pp. 53–54, 2000.

[9] N. G. R. Broderick, T. M. Monro, P. J. Bennett, and D. J. Richardson, "Nonlinearity in holey optical fibers: Measurement and future opportunities," *Opt. Lett.*, vol. 24, pp. 1395–1397, 1999; *Opt. Lett.*, vol. 24, no. 20, p. 1647, 1999.

[10] B. J. Eggleton, P. S. Westbrook, C. A. White, C. Kerbage, R. S. Windeler, and G. L. Burdge, "Cladding-mode-resonances in air-silica microstructure optical fiber," *J. Lightwave Technol.*, vol. 18, no. 8, pp. 1084–1100, 2000.

[11] A. Ortigosa-Blanch, J. C. Knight, W. J. Wadsworth, J. Arriaga, B. J. Mangan, T. A. Birks, and P. St. J. Russell, "Highly birefringent photonic crystal fibers," *Opt. Lett.*, vol 25, no. 18, pp. 1325–1327, 2000.

[12] B. H. Lee, J. B. Eom, J. Kim, D. S. Moon, U.-C. Paek, and G.-H. Yang, "Photonic crystal fiber coupler," *Opt. Lett.*, vol. 27, no. 10, pp. 812–814, 2002.

[13] J. K. Ranka, R. S. Windeler, A. J. Stentz, "Visible continuum generation in air-silica microstructure optical fibers with anomalous dispersion at 800 nm," *Opt. Lett.*, vol. 25, no. 1, pp. 25–27, 2000.

[14] S. Coen, A. H. L. Chau, R. Leonhardt, J. D. Harvey, J. C. Knight, W. J. Wadsworth, P. St. J. Russell, "White-light supercontinuum generation with 60-ps pump pulses in a photonic crystal fiber," *Opt. Lett.*, vol. 26, no. 17, pp. 1356–1358, 2001.

[15] A. K. Varshneya, *Fundamentals of inorganic glasses* (Academic press, New York, 1994).

[16] Y. Dogu, and D. A. Kaminski, "Effects of eccentricity on glass temperature in the neck-down stage of the optical fiber drawing process," Proceedings of the ASME Heat Transfer Division, vol. 1, pp. 89–100, 1997.

[17] T. Sorensen, J. Broeng, A. Bjarklev, E. Kundsen, and E. E. Barkou Libori, "Macro-bending loss properties of photonic crystal fibre," *Electron. Lett.*, vol. 37, no. 5, pp. 287–288, 2001.

[18] J. C. Knight, T. A. Birks, P. St. J. Russell, and J. P. de Sandro, "Properties of photonic crystal fiber and the effective index model," *J. Opt. Soc. Am. A*, vol. 15, no. 3, pp. 748–752, 1998.

[19] M. C. Carlson, "Measuring Polarization-Dependent Loss with the IQ-12004B DWDM Passive Component Test System," EXFO Application Note, ANOTE050.1AN, 2001, http://documents.exfo.com/appnotes/anote050an.pdf.